

An Unsteady Long Bearing Squeeze Film Damper Model Part II: Statically Eccentric Operation

P. A. Schallhorn, D. A. Elrod, D. G. Goggin, A. K. Majumdar

Sverdrup Technology, Inc.
Huntsville, Alabama 35806

ABSTRACT

This paper, the second of a two-part series, presents results of an unsteady rotordynamic analysis of a long-bearing squeeze film damper executing orbits about an off center position using a fluid circuit approach. A series of nodes and branches represent the geometry of the flow circuit. The mass and momentum conservation equations are solved to predict the pressure distribution in the squeeze film. The motion of the bearing is simulated by the variation of geometry within the flow path. This effort represents the first modeling approach which allows for an arbitrary orbit size about an arbitrary position.

Nomenclature

- C Squeeze film damper radial clearance (difference in radii)
- $C_p = \mu\omega R^2/C^2$ Pressure conversion factor
- $C_{tt} = -f_t/\epsilon$ Dimensionless direct damping coefficient
- d Damper journal diameter

D_r	$= f_r/\epsilon$	Dimensionless direct inertia coefficient
e		Dynamic eccentricity (orbit radius)
L		Damper journal length
\dot{m}		Mass flow rate
p		Local pressure within the squeeze film region
r		Radial coordinate
R		Damper journal radius
Re	$= \rho\omega C^2/\mu$	Reynolds number
z		Axial coordinate
ϵ	$= e/C$	Eccentricity ratio (dimensionless orbit radius)
θ		Circumferential coordinate
μ		Fluid absolute viscosity
ρ		Fluid density
τ_f		Shear stress
ω		Frequency of damper journal (whirl frequency)

Introduction

In the first paper (Part I), all models considered a circular centered orbit, i.e. the orbit of the bearing about the center of the housing. Steady state methods have been used to predict the squeeze film forces to varying degrees of success for these circular centered orbits. Once the center of the orbit is eccentric (the center of the bearing

orbit is about some point other than the center of the housing) an unsteady solution is required for all but extremely small orbit size cases since no coordinate transformation can result in a constant geometry for this situation. An unsteady model of the damper was therefore needed. The first paper in this two part series (Part I) developed the basis for the unsteady solution and benchmarked the technique against published experimental results². This paper presents the results of a modeling effort for eccentric operation of a squeeze film damper executing a large orbit (Figure 1 illustrates schematically the eccentric operation of a squeeze film damper). These results are the first available for this situation, either analytical or experimental, and represent a significant improvement in the state-of-the-art.

Fluid Flow Code

A general purpose, one-dimensional, network flow analysis computer code was chosen as the platform for SFD modeling¹⁰. The code uses a series of nodes and branches to define a flow network. Nodes are positions within the network where fluid properties (pressure, density, etc.) are either known or calculated. Branches are the portions of the flow network where flow conditions (geometry, flow rate, etc.) are known or calculated. The code uses a finite volume approach with a staggered grid. This approach is commonly used in computational fluid dynamics schemes (Patankar¹⁵, Patankar and Karki¹⁶). The staggered grid approach uses overlapping control volumes where the conservation of mass and the conservation of momentum are calculated in separate control volumes. For a conventional grid where only one

control volume is used for both scalar and vector quantities, interpolation is required in formulating the conservation of the scalar quantities at the edges of the control volume and numerical errors result. For a staggered grid, however, mass flow rates are available at the surface of the continuity control volume and do not have to be interpolated.

Unsteady Long Bearing Squeeze Film Damper Modeling

The geometry of the damper is assumed to be that of the circular centered orbit benchmark case given by Jung, *et al*². The inner race of the bearing has a radius of 2.5 inches, is 0.94 inches long, has a clearance of 0.0625 inches and is fully sealed on one end, mostly sealed on the other end. As in the first paper of this series (Part I), the bearing remains wrapped (see Figure 2); however, curvature is neglected since the clearance to radius ratio is small ($\sim 1/40$). The motion of the inner race of the damper is simulated by the variation of the geometry of the flow path, as is illustrated in Figure 3. This geometry variation generates a pressure variation around the circumference of the damper. For rotordynamics applications, the pressure distribution of the fluid circuit model is integrated to obtain the radial and tangential forces of Equations 1 and 2.

$$F_r = \int_0^{2\pi} p A_{\text{normal}} \cos\theta d\theta \quad (1)$$

$$F_t = \int_0^{2\pi} p A_{\text{normal}} \sin \theta d\theta \quad (2)$$

In a dimensionless form, the radial and tangential forces are calculated using Equations 3 and 4, where C_p is the pressure coefficient defined in the nomenclature.

$$f_r = \int_0^{2\pi} \frac{p}{C_p} \cos \theta d\theta \quad (3)$$

$$f_t = \int_0^{2\pi} \frac{p}{C_p} \sin \theta d\theta \quad (4)$$

In rotordynamic models, these force components are represented by rotordynamic coefficients. These coefficients are analogous to the mass, damping and stiffness terms for a spring-mass-damper system. For an uncavitated squeeze film damper, the only two coefficients which occur are a radial inertia (or added mass) term, D_{rr} , and a circumferential damping term, C_{tt} . In order to compare with published experimental results², the damping and inertia coefficients are normalized by the eccentricity ratio and pressure coefficient, equations 5 and 6. Equation 5 is the non-dimensional circumferential damping coefficient and Equation 6 is the non-dimensional radial inertia coefficient.

$$C_{tt} = -f_t/\varepsilon \quad (5)$$

$$D_{rr} = f_r/\epsilon \quad (6)$$

Results

Initial Eccentric Squeeze Film Damper Model

The initial eccentric SFD model uses an orbit eccentricity ratio of $\epsilon = 0.4$ about an off-center position described by a “static” eccentricity ratio of $\epsilon_s = 0.4$. Figure 3 illustrates the clearance versus node number for four positions within the orbit (corresponding to $\omega t = 0$ & 2π , $\pi/2$, π , and $3\pi/2$ radians). The pressure has been non-dimensionalized using equation 16 for comparison with Jung’s published data.

$$\frac{p}{p_{\text{reference}}} = \frac{p}{C_p \text{Re}} = \frac{p}{\rho R^2 \omega^2} \quad (11)$$

Pressure results are provided in Figure 4. As the pressure wave propagates it also deforms in contrast to the centered case (Part I, Figure 4). Since the pressure wave deforms, the radial and tangential forces are functions of position in the orbit (i.e. the coefficients are periodic functions of time). This leads to rotordynamic system modeling questions beyond the scope of this work, such as: Should time averaged coefficients be used when encountering eccentric operation, or should the coefficients be modeled as periodic in time? Do time dependent rotordynamic coefficients make sense, or do time dependent radial and tangential forces make more sense? It is the opinion of this author that until rotordynamic system level codes are modified to

handle modeling periodic forces at squeeze film damper locations, time averaged coefficients should be used with the understanding that these values represent only the mean value. Once the rotordynamic codes have been modified, the actual periodic force components should then be used.

Figure 5 shows the difference in the dimensionless pressure profiles between the centered and eccentric operation at the position in the orbit of the eccentric case where absolute minimum clearance is attained. The velocity of the damper inner segment between the two cases is dramatically different (the damper inner segment velocity for the statically eccentric case is less than 50% of velocity for the centered case). This velocity difference is reflected in their respective dimensionless pressure magnitudes. Note that the absolute minimum clearances between these two cases differ slightly (the centered case has a minimum clearance of 0.01125 inches whereas the eccentric case has an absolute minimum clearance of 0.0125 inches).

Eccentric Operation Parametric Studies

Upon the success of the initial eccentric model, a parametric study was conducted on the predicted SFD performance. The study examined the variation in both orbit size and static eccentricity for Reynolds number of 49.0. The dynamic eccentricity ratios (ϵ_d , dimensionless orbit size) examined in the study ranged from 0.2 to 0.4. The static eccentricity ratios, ϵ_s , examined in the study ranged from 0.2 to 0.6. (Refer to Figure 5b as reference to statically eccentric operation).

The results of the study are provided in Figures 6 through 13. Figures 6 and 7 provide the results for a dynamic eccentricity ratio of 40% ($\epsilon_d = 0.4$) for two static eccentricity ratios ($\epsilon_s = 0.2$ and $\epsilon_s = 0.4$). These figures show the effect of static offset on the results for a moderate orbit size. As these two figures indicate, as the static eccentricity increased the forces on the rotor increase and the force profile becomes asymmetric. These observations are not unexpected as the influence of the housing increases as the static eccentricity increases. One other notable observation is that the radial (inertia) force component is larger than the tangential (damping) force component.

Figures 8 and 9 show the effect of orbit size for a small static offset. The static eccentricity is at 20% ($\epsilon_s = 0.2$) and the orbit size ranges from 20% - 60% ($\epsilon_d = 0.2 - 0.6$). These figures show that an increase in the orbit size results in an increase in the force components. Note that as the orbit size decreases, the effect of the small static offset diminishes and the force components are nearly constant over one period.

Figures 10 and 11 show the effect of orbit size for a moderate static offset. The static eccentricity is at 40% ($\epsilon_s = 0.4$) and the orbit size ranges from 20% - 40% ($\epsilon_d = 0.2 - 0.4$). Note that unlike the small static offset case, the effect of the moderate static offset does not diminish to the point where the force components are nearly constant over one period (as orbit size decreases).

One final parametric study was conducted to examine the effect of Reynolds number on eccentric behavior. The study used a single static eccentricity and dynamic eccentricity. The eccentricities were both set at 40% ($\epsilon_s = \epsilon_d = 0.4$). The results of the study are presented in Figures 12 and 13. The predictions indicate that the Reynolds number has a major influence on the radial force (inertia force), but a lesser influence on the tangential force (damping force). This may indicate that for a moderately offset condition, damping is controlled more by the offset than by the operating speed; whereas inertia is still controlled by fluid inertia.

Conclusions

This study successfully demonstrates unsteady modeling of orbits about a statically eccentric position. The results not only provide proof of concept for such predictions (only an unsteady model can provide such predictions), they also provide insight into the behavior of the pressure field for this mode of squeeze film damper operation. Additionally, the results indicate that either mean values of the rotordynamic coefficients are needed in current rotordynamic models or that rotordynamic models will need to be modified (e.g., models must be able to handle either time dependent/periodic coefficients or time dependent/periodic forces).

Two parametric studies were conducted on statically eccentric operation. The first study examined the effect of static eccentricity for given orbit sizes at a Reynolds number of 49. The results indicate that as the static eccentricity increases, the forces over a period become asymmetric. For a small orbit size ($\epsilon_d \sim 0.2$), the effect of static offset diminishes and the force components are nearly constant over one period (i.e. for a small static offset, say $\epsilon_s \sim 0.2$, the effect of the offset becomes negligible); however, for moderate orbit size ($\epsilon_d \sim 0.4$), the effect of a small offset cannot be neglected. For all cases examined in this study, the radial force (inertia force) was always predicted to be greater than the tangential force (damping force).

A second parametric study examined the effect of Reynolds number on statically eccentric operation. The static and dynamic eccentricities for the study were each set at 40% ($\epsilon_s \sim 0.4$ and $\epsilon_d \sim 0.4$). The study indicated that the radial force (inertia force) was highly sensitive to Reynolds number; however, the tangential force (damping force) was not as sensitive. This may indicate that for a moderately offset condition, damping is controlled more by the offset than by the operating speed; whereas inertia is still controlled by fluid inertia.

In conclusion, it must be recognized that this study successfully demonstrated a technique for modeling a squeeze film damper executing an arbitrary orbit radius about an arbitrary position. In order to validate the predictions presented, an experimental investigation is necessary.

Acknowledgments

The work was performed for the National Aeronautics and Space Administration's Marshall Space Flight Center under Task Directive 611-022 for Contract NAS8-40836 with Mr. Eric Earhart as the Task Initiator. The authors would like to acknowledge the support of Dr. Steven Ryan of the Marshall Space Flight Center and Dr. Robert LeMaster of Sverdrup Technology.

References

1. Jung, S.Y.; San Andres, L.A.; Vance, J.M.: "Measurements of Pressure Distributions and Force Coefficients in a Squeeze Film Damper Part I: Fully Open Ended Configuration," *Tribology Transactions*, Volume 34, No. 3, pp. 375-382, 1991.
2. Jung, S.Y.; San Andres, L.A.; Vance, J.M.: "Measurements of Pressure Distributions and Force Coefficients in a Squeeze Film Damper Part II: Partially Sealed Configuration," *Tribology Transactions*, Volume 34, No. 3, pp. 383-388, 1991.
3. San Andres, L.A.: "Effect of Fluid Inertia on Force Coefficients for the Long Squeeze Film Damper," *Tribology Transactions*, Vol. 31, No. 3, pp. 370-375, 1988.

4. San Andres, L.A; Vance, J.M.: "Effect of Fluid Inertia on the Performance of Squeeze Film Damper Supported Rotors," *ASME Journal of Engineering for Gas Turbines and Power*, Vol. 110, pp. 51-57, January 1988.
5. San Andres, L.A; Vance, J.M.: "Effect of Fluid Inertia on Squeeze-Film Damper Forces for Small-Amplitude Circular-Centered Motions," *ASLE Transactions*, Vol. 30, No. 1, pp. 62-68, 1987.
6. San Andres, L.A; Vance, J.M.: "Effect of Fluid Inertia and Turbulence on the Force Coefficients for Squeeze-Film Dampers," *ASME Journal of Engineering for Gas Turbines and Power*, Vol. 108, pp. 332-339, April 1986.
7. Tichy, J.A.: "A Study of the Effect of Fluid Inertia and End Leakage in the Finite Squeeze Film Damper," *ASME Journal of Tribology*, Vol. 109, pp. 54-59, January 1987.
8. Tichy, J.A.: "Effects of Fluid Inertia and Viscoelasticity on the One-Dimensional Squeeze-Film Bearing," *ASLE Transactions*, Vol. 27, No. 2, pp. 164-167, 1984.
9. Tichy, J.A.: "Effects of Fluid Inertia and Viscoelasticity on Squeeze-Film Bearing Forces," *ASLE Transactions*, Vol. 25, No. 1, pp. 125-132, 1982.

10. Majumdar, A.K.: "A Generalized Fluid System Simulation Program to Model Flow Distribution in Fluid Networks," SvT Report No. 331-201-96-003, October 1996.
11. Vance, J.M.: Rotordynamics of Turbomachinery, pp. 240-247, J. Wiley & Sons, 1988.
12. Schallhorn, P.A.; Elrod, D.A.; Goggin, D.G.; Majumdar, A.K.: "A Fluid Circuit Model for Long Bearing Squeeze Film Damper Rotordynamics," *AIAA Journal of Propulsion and Power*, submitted for consideration of publication December, 1998.
13. Schallhorn, P.A.: Unsteady Analysis of the Fluid Film Forces in a Long Bearing Squeeze Film Damper, Ph.D. Dissertation, The University of Alabama in Huntsville, 1998.
14. Schallhorn, P.A.: "Unsteady Long Bearing Squeeze Film Damper Modeling for Circular Centered Orbits and Statically Eccentric Operation," SvT Report No. 611-022-98-002, November 1998.
15. Patankar, S., *Numerical Heat Transfer and Fluid Flow*, Hemisphere Publishing Co., New York, 1980.

16. Patankar, S., Karki, K., *Documentation of COMPACT-2D Version 3.1*, (User's Manual) Innovative Research, Inc., 1993.

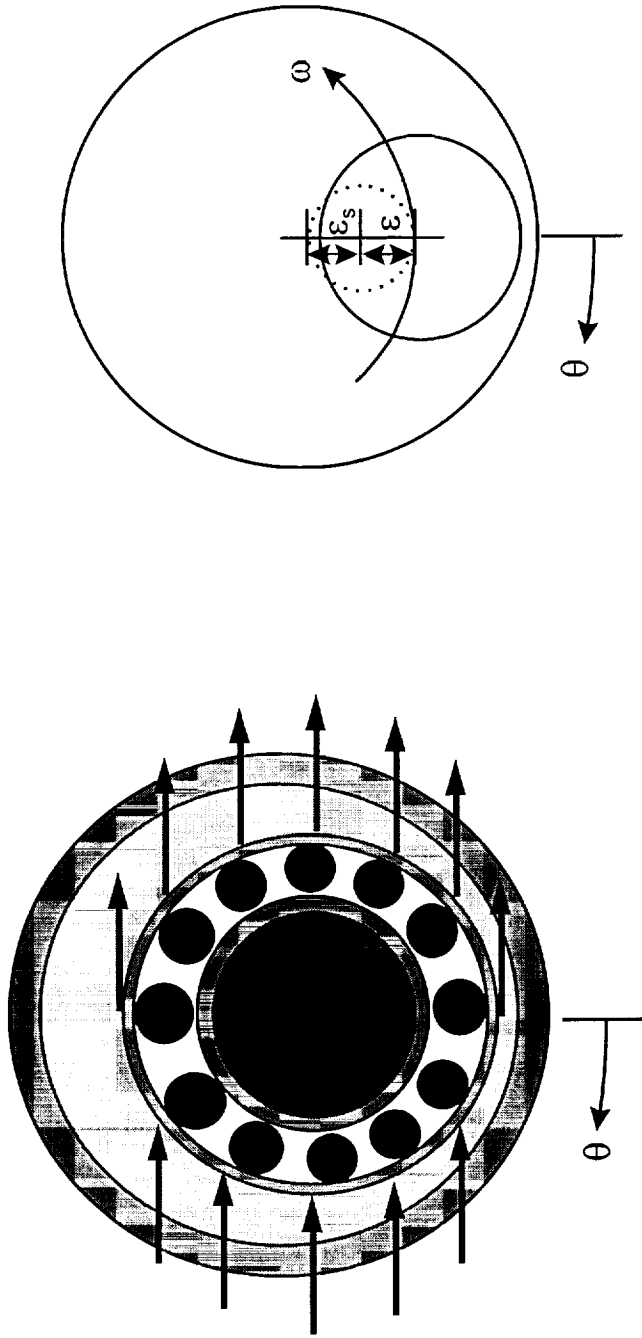


Figure 1: Schematic of Orbit About A Statically Eccentric Position

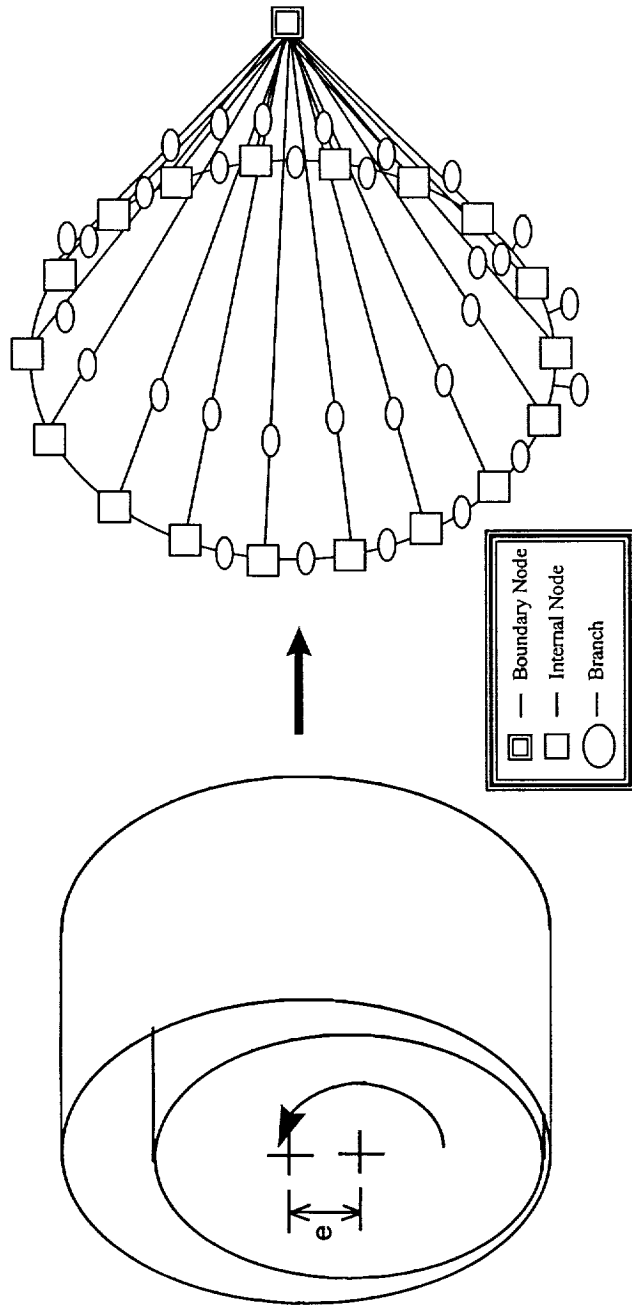


Figure 2: Unsteady Squeeze Film Damper Modeling

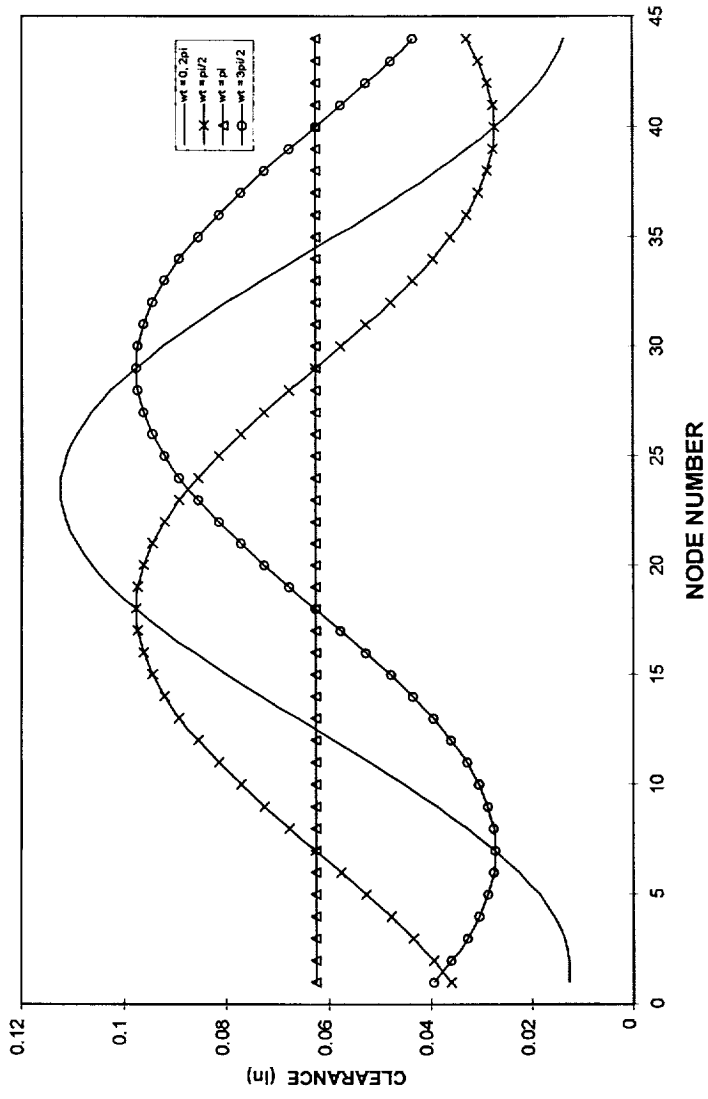


Figure 3: Unsteady Squeeze Film Damper Modeling Geometry Variation for Orbits

About an Eccentric Position

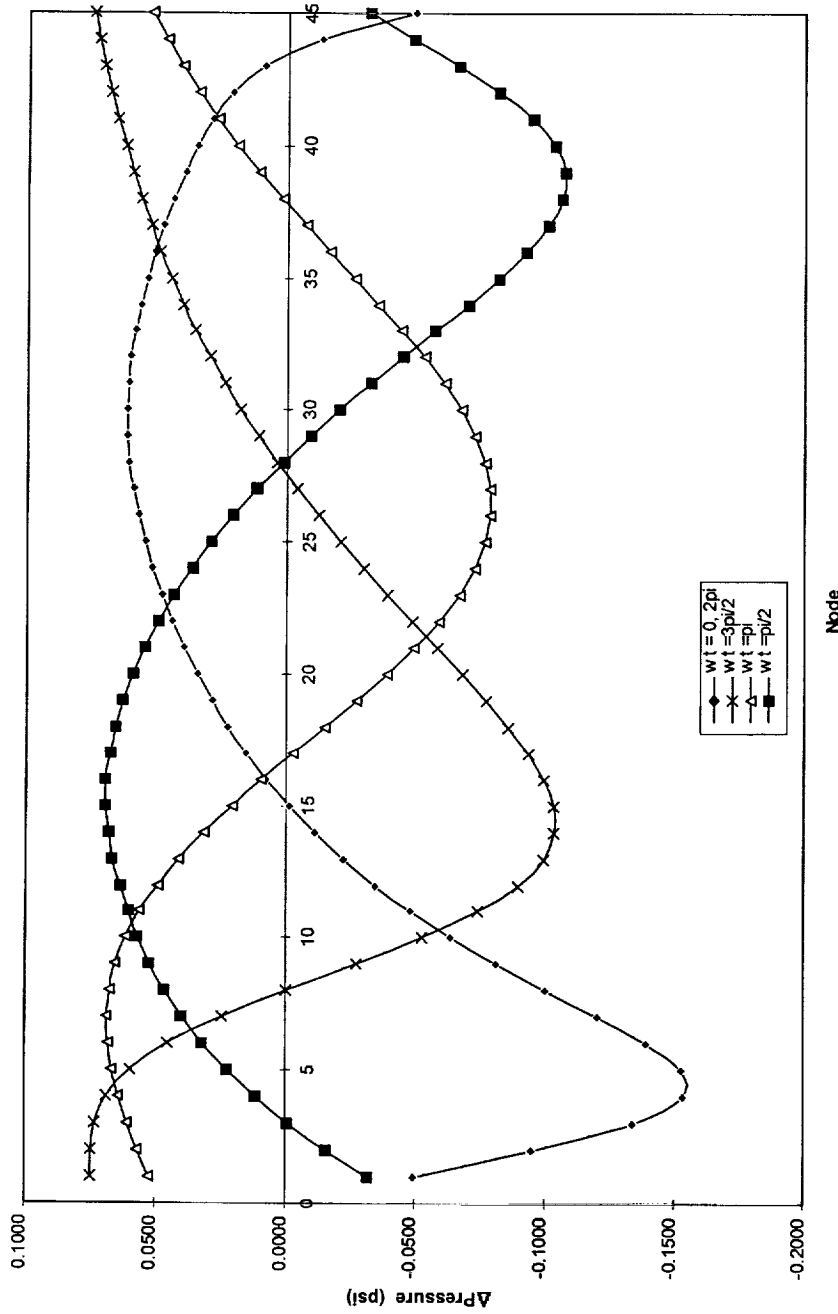
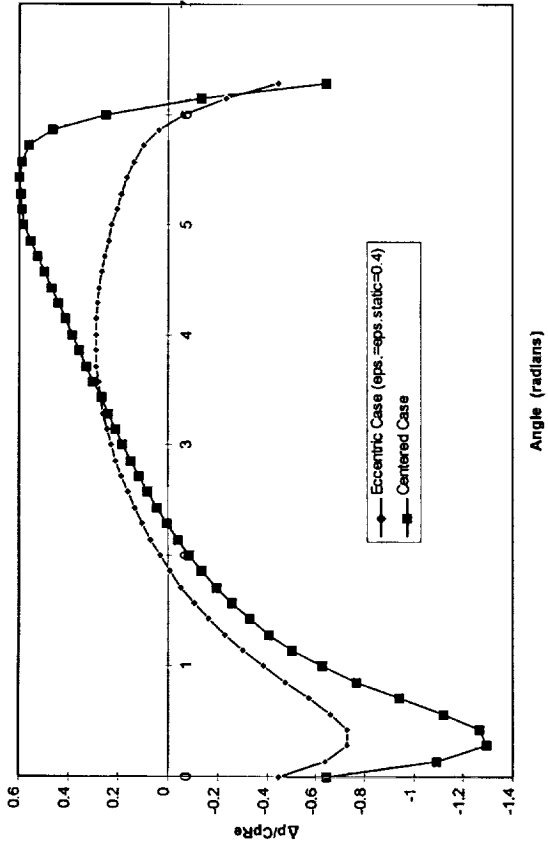
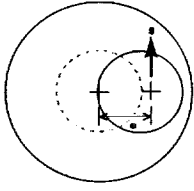


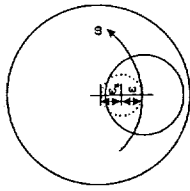
Figure 4: GFSSP Predicted Pressure Profile for Eccentric Operation Initial Model



(a)



Centered Case



Eccentric Case @ $\omega t=0$

(b)

Figure 5: GFSSP Predicted Pressure Profile Comparison: Circular Centered Orbit vs. Orbit About a Statically Eccentric Position

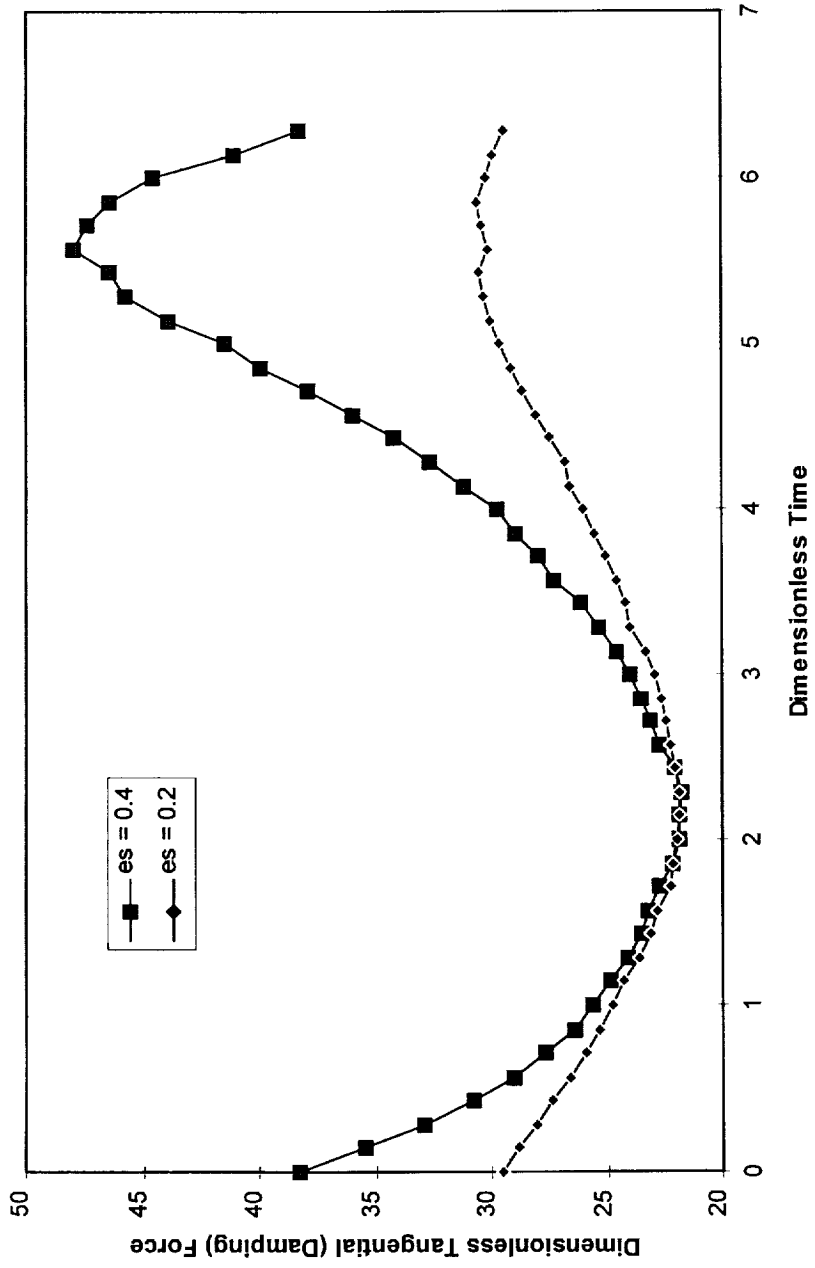


Figure 6: Dimensionless Tangential (Damping) Force vs. Dimensionless Time for $\epsilon_d = 0.4$, $Re = 49.0$

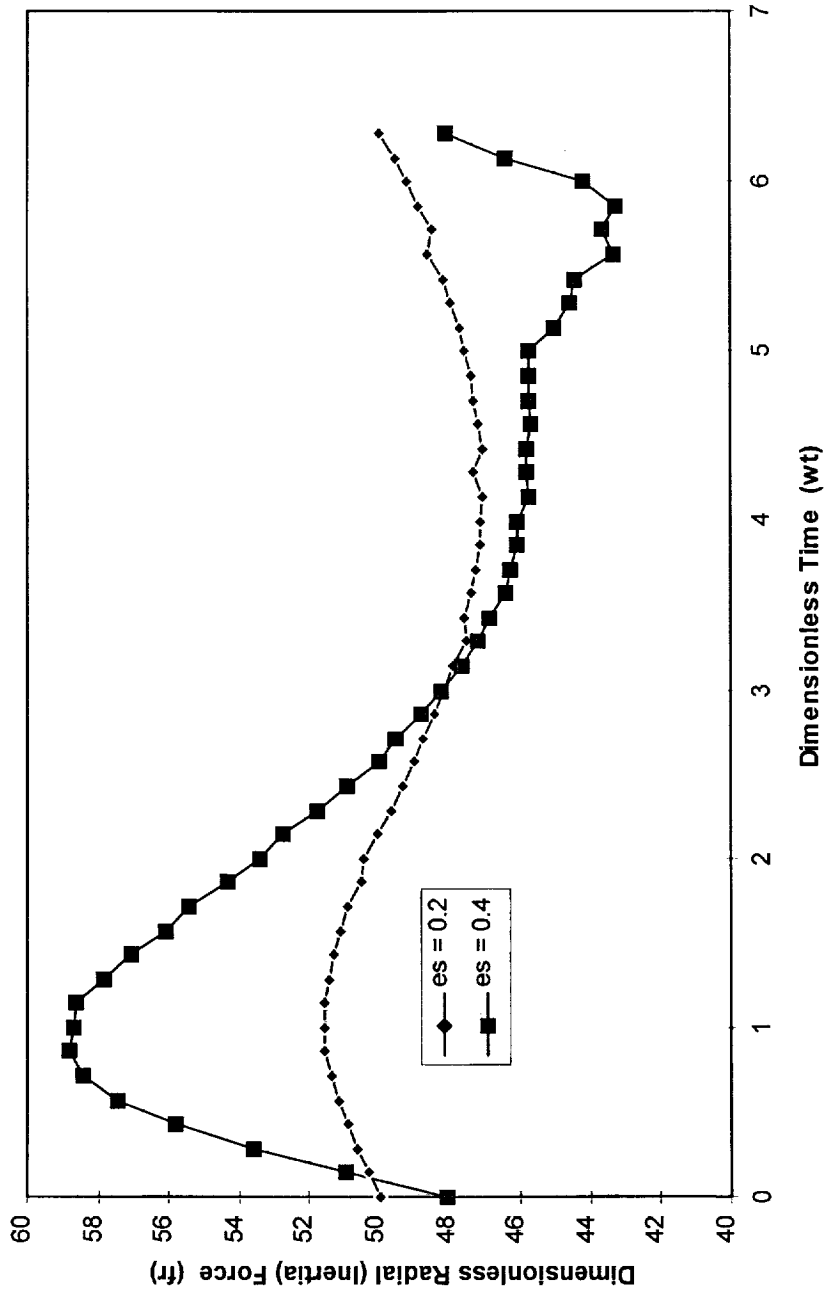


Figure 7: Dimensionless Radial (Inertia) Force vs. Dimensionless Time for $\epsilon_d = 0.4$, $Re = 49.0$

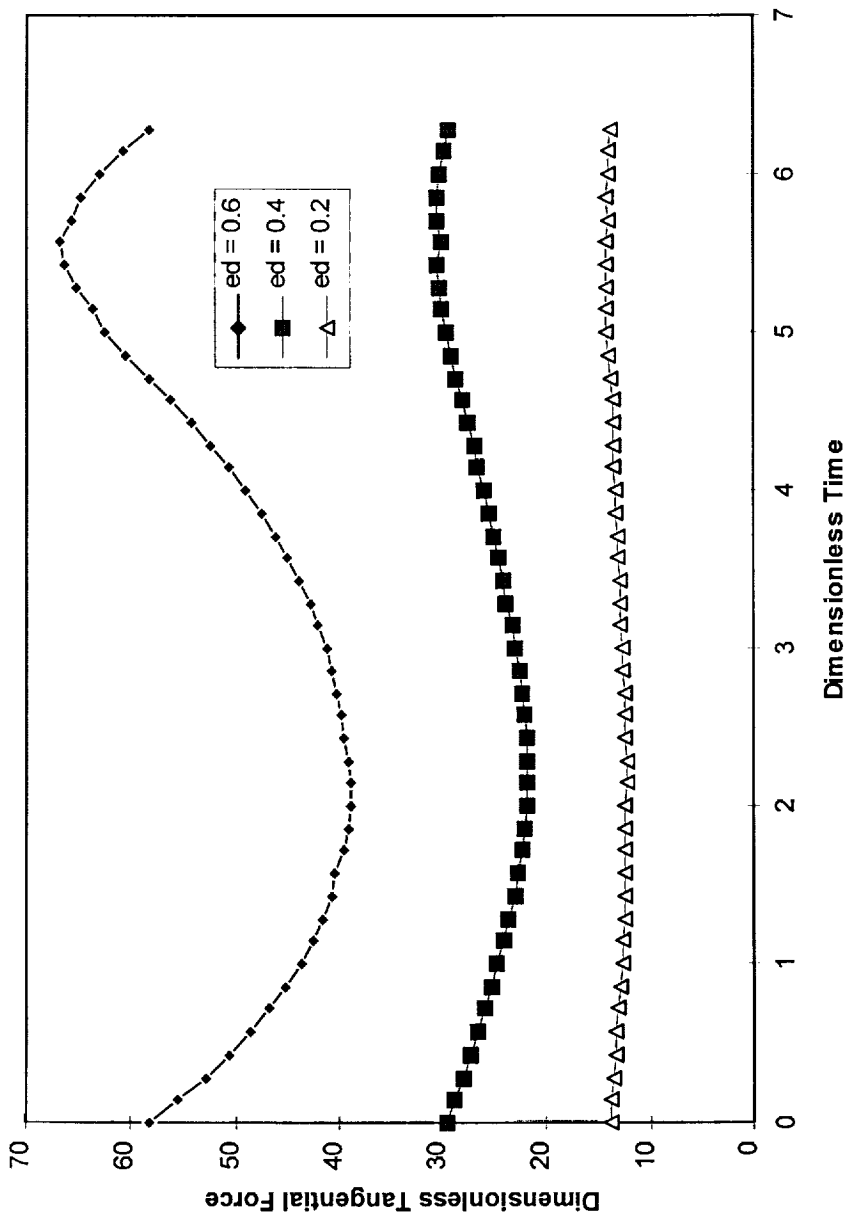


Figure 8: Dimensionless Tangential (Damping) Force vs. Dimensionless Time for $\varepsilon_s = 0.2, Re = 49.0$

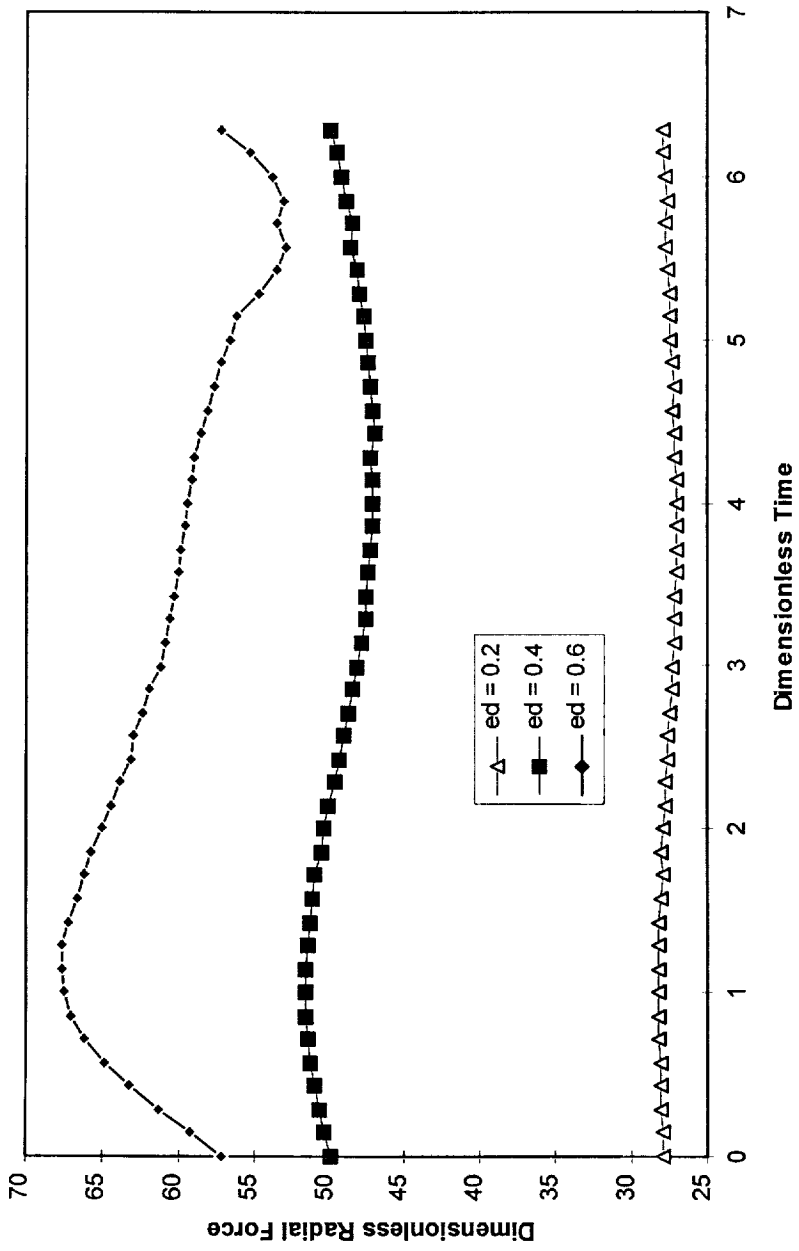


Figure 9: Dimensionless Radial (Inertia) Force vs. Dimensionless Time for $\epsilon_s = 0.2$, $Re =$

49.0

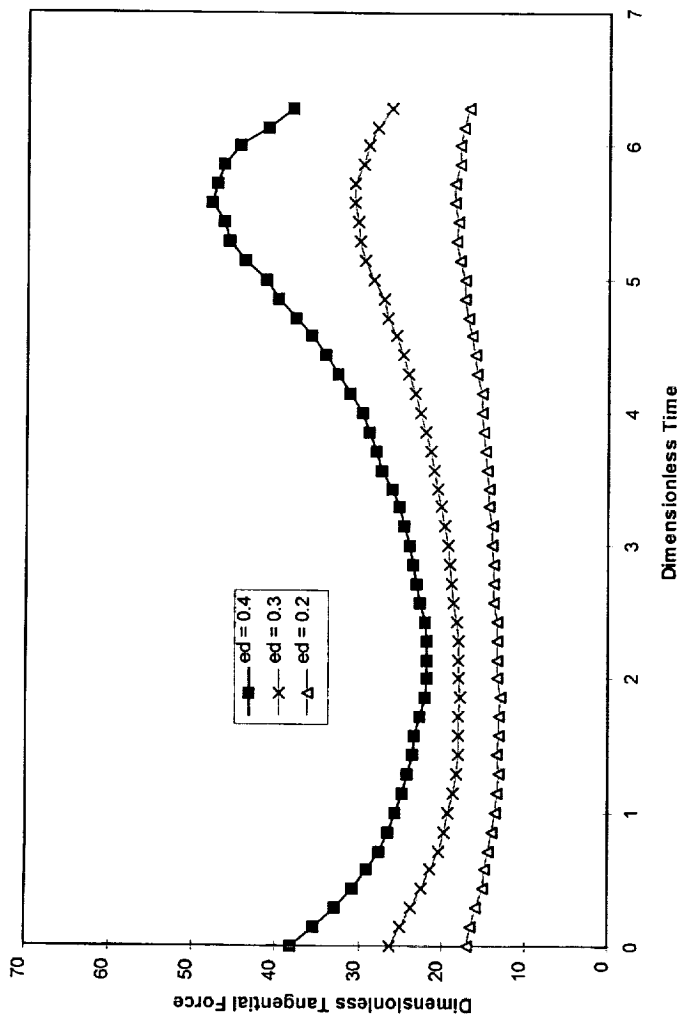


Figure 10: Dimensionless Tangential (Damping) Force vs. Dimensionless Time for $\varepsilon_s = 0.4$, $Re = 49.0$

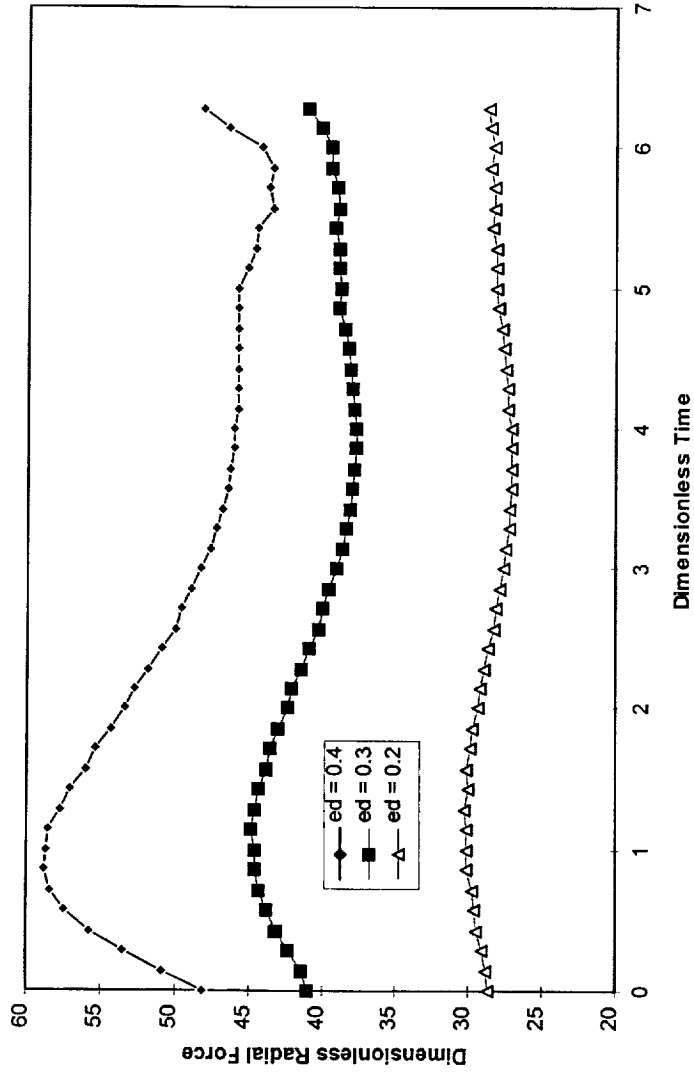


Figure 11: Dimensionless Radial (Inertia) Force vs. Dimensionless Time for $\varepsilon_s = 0.4$, $Re = 49.0$

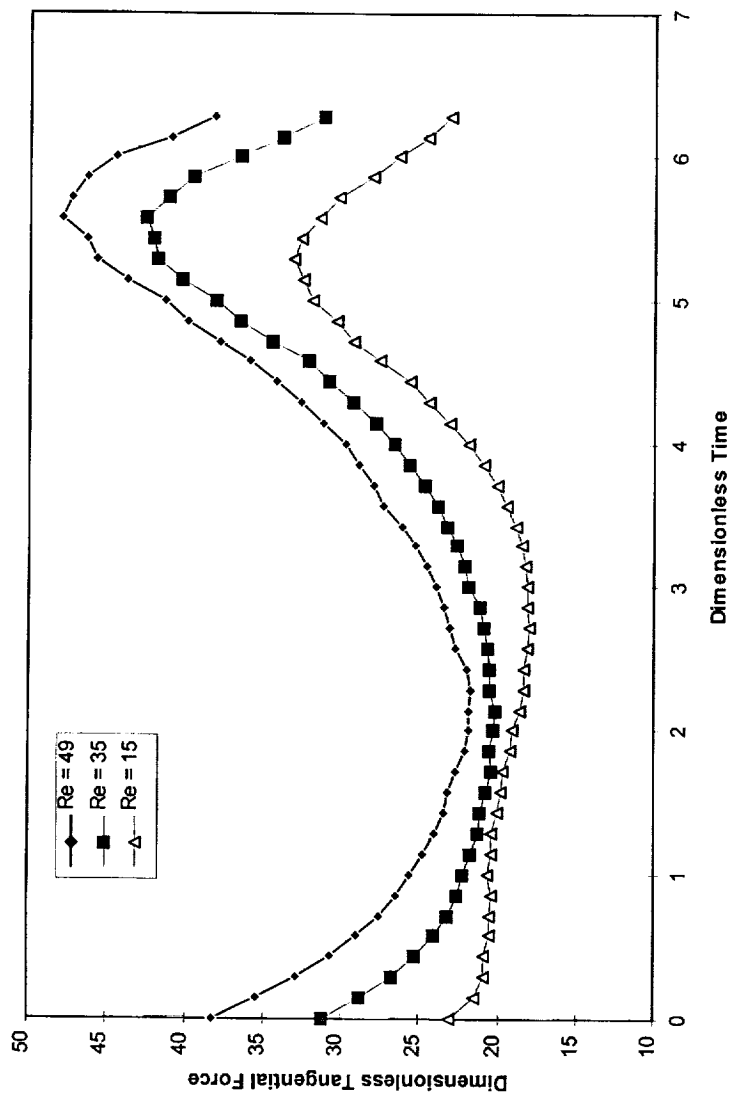


Figure 12: Dimensionless Tangential (Damping) Force vs. Dimensionless Time for $\epsilon_s = \underline{\epsilon_d = 0.4}$

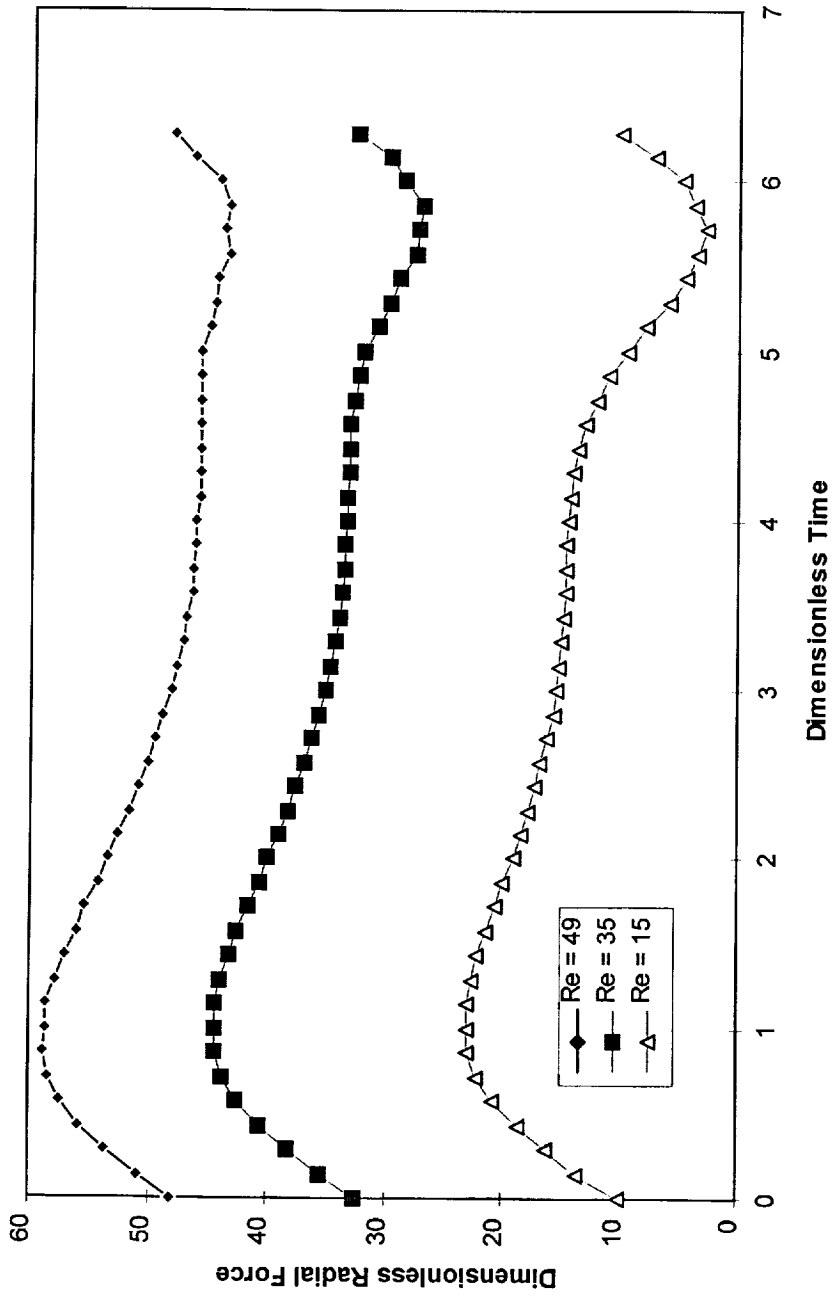


Figure 13: Dimensionless Radial (Inertia) Force vs. Dimensionless Time for $\epsilon_s = \epsilon_d = 0.4$